Journal of Applied Physics

RESEARCH ARTICLE | FEBRUARY 11 2026

The mechanism of hydroxyapatite coatings degradation at high substrate temperatures

Salizhan Kylychbekov ; Bektur Abdisatarov ; Yaran Allamyradov ; Berdimyrat Annamuradov ; Liviu Duta ; Ali Oguz Er

J. Appl. Phys. 139, 065304 (2026)
https://doi.org/10.1063/5.0297660

AIP Publishing

Journal of Applied Physics ARTICLE pubs.aip.org/aip/jap

The mechanism of hydroxyapatite coatings degradation at high substrate temperatures

Cite as: J. Appl. Phys. **139**, 065304 (2026); doi: 10.1063/5.0297660
Submitted: 20 August 2025 · Accepted: 3 January 2026 ·
Published Online: 11 February 2026

Salizhan Kylychbekov,[1] Bektur Abdisatarov,[2] Yaran Allamyradov,[3] Berdimyrat Annamuradov,[3] Liviu Duta,[4] and Ali Oguz Er[3,a)]

AFFILIATIONS

[1]Department of Materials, University of Oxford, Parks Road, Oxford OX1 3PH, United Kingdom
[2]Superconducting Quantum Materials and Systems Center, Fermi National Accelerator Laboratory (FNAL), Batavia, Illinois 60510, USA
[3]Department of Physics and Astronomy, Western Kentucky University, Bowling Green, Kentucky 42101, USA
[4]Lasers Department, National Institute for Laser, Plasma and Radiation Physics, Magurele 077125, Romania

[a)]**Author to whom correspondence should be addressed:** ali.er@wku.edu

ABSTRACT

Physical vapor deposition methods used for hydroxyapatite (HA) coatings typically require elevated substrate temperatures and post-deposition annealing to induce crystallization. However, such thermal treatments can degrade both the mechanical integrity and bioactivity of the coating, particularly when substrate temperatures exceed 500 °C. The mechanisms underlying these phenomena remain insufficiently understood. In this study, HA thin films were deposited on silicon and Ti6Al4V substrates using pulsed laser deposition and were systematically characterized to elucidate these mechanisms. XPS and SIMS analyses revealed a temperature-dependent loss of OH^- and PO_4^{3-} groups, an increased Ca/P ratio, and the formation of interfacial oxides, all of which contribute to weakened adhesion. To clarify the temperature-dependent decline in bioactivity, protein adsorption behavior was analyzed using a Kramers-type kinetic framework; the fitted desorption kinetics indicate that coatings deposited near ~500 °C provide the most stable protein attachment, whereas higher temperatures accelerate desorption due to dehydroxylation and carbonate substitution. Together, these findings provide mechanistic insight into the thermal degradation of HA coatings and offer a framework for optimizing deposition parameters to preserve stoichiometry, adhesion, and bioactivity for long-term biomedical applications.

I. INTRODUCTION

Metallic implants (stainless steel 316L, Co–Cr, and Ti alloys) provide strength and corrosion resistance, but lack intrinsic bioactivity, which can impede osseointegration and complicate healing.[1,2] Improving the tissue–implant interface with bioactive coatings is therefore critical for clinical performance. The inorganic biomaterial hydroxyapatite [HA, $Ca_{10}(PO_4)_6(OH)_2$], with a calcium-to-phosphorus (Ca/P) ratio of 1.67, is widely used because its composition and ion-exchange behavior closely resemble bone mineral, supporting osteoconductivity, biocompatibility, and controlled resorption.[3–6] Additional functionalities such as osteoinductivity can be engineered through strategies like ion-substitution.[7] However, coating non-degradable and functional HA films poses a significant challenge because amorphous films and other calcium phosphate (CaP) phases tend to decompose over time in saline human body environment.[8]

Numerous deposition routes exist for HA coatings [plasma spray, sputtering, pulsed laser deposition (PLD), chemical/electrodeposition, and hybrids], each with characteristic trade-offs in crystallinity, phase purity, adhesion, and processing temperature. However, each method presents characteristic limitations or challenges inherent to its processing parameters. Achieving a uniform and crystalline coating with high surface adhesion using this technique is very challenging. Dip coating is a straightforward technique for applying HA coatings on metallic materials. However, it has a critical flaw—poor bonding strength of HA to the metal surface. Additionally, amorphous HA coatings are soluble in the human body and brittle under deformation,[9] whereas crystalline films offer better mechanical fatigue resistance and are stable in implants.[10]

Among these, PLD enables near-stoichiometric transfer and fine control of ambient conditions, fluence, and substrate temperature, yielding dense coatings with good adhesion.[11–14] Many studies report that *in situ* and post-deposition annealing at elevated temperatures (above 400 °C) is a necessary step to achieve crystalline HA, which promotes stability in human body fluids.[15,16]

In PLD, as well as in sputtering or molecular beam evaporation systems, high substrate temperatures are typically employed to promote film crystallinity and adhesion. This leads to issues such as the degradation of HA into other Ca–P phases that are far less stable compared to HA.[17] Numerous studies have reported the transition from HA to α- and β-tricalcium phosphate (TCP), tetracalcium phosphate (TTCP), and other unwanted phases of CaPs that are far less stable in the human body environment compared to HA.[15,16,18] In fact, previous studies revealed that the order of relative solubility of CaPs is as follows: ACP $\gg$ DCP $>$ TTCP $>$ $\alpha-$TCP $>$ $\beta-$TCP $\gg$ HA,[19–21] where ACP and DCP are abbreviations for amorphous and dicalcium phosphate. Among all phases, the crystalline phase of HA exhibits the highest stability while keeping its main bioactive and biocompatibility properties,[15] unlike the amorphous phase.

The obtaining of crystalline HA typically involves thermal treatment. However, in our previous work, we observed a decline in bioactivity, cell proliferation, and structural properties of HA coatings at elevated substrate temperatures.[17] Addressing these issues is essential for producing HA coatings that comply with ISO standards.[22–24] Therefore, a thorough understanding of the underlying chemical and physical mechanisms is necessary for optimizing coating performance.

While HA coatings by PLD onto metallic substrates exploring their crystallinity, adhesion, composition, or *in vitro* bioactivity under various conditions have been extensively studied,[25–27] none of them gave conclusive answers to what kind of mechanisms are involved in the degradation of adhesion and bioactivity properties, apart from possible hypotheses or description of partial processes. This work tackles the problem through temperature-resolved mechanistic dissection of how thermal deposition conditions degrade HA film integrity and adhesion. We combined elemental and phase analysis methods in XPS, EDS, and XRD with SIMS depth profiling across a broad temperature range, room temperature (RT) to 800 °C, to elucidate (i) the compositional drift (loss of volatile OH^- and PO_4^{3-} species), (ii) the emergence of interfacial oxide/diffusion layers, and (iii) the coupling between compositional, structural, and interfacial changes leading to adhesion loss. This mechanistic linkage across multiple scales has not been systematically elaborated previously. Furthermore, the aim of this study was also motivated by the decline in bioactivity and mechanical performance noted in our recent work,[17] which aligns with common observations from other groups as well. To conclude, HA coatings improve the properties of AZ31B alloys, but only up to 200 °C. Beyond this threshold, mechanical properties and corrosion resistance are no longer maintained.[28]

Overall, a detailed understanding of these degradation mechanisms provides the foundation for addressing the specific factors needed to produce high-quality HA coatings suitable for industrial-standard implant applications.

II. MATERIALS AND METHODS

A. HA coating

HA thin films were deposited onto Si(100) and Ti6Al4V (Grade 5) substrates. Ti6Al4V coupons ($\approx 15 \times 15\ mm^2$) were mechanically polished (SiC to 1000 grit, then 0.05 μm colloidal silica/alumina) and solvent-cleaned prior to loading. Depositions were performed in UHV (base pressure $\sim 10^{-8}$ Torr; working pressure $\sim 10^{-6}$ Torr) using a rotating dense HA target. A nanosecond Nd:YAG source operated at 532 nm, 5 ns, 10 Hz with fluence $\sim 7.4\ J\ cm^{-2}$; the beam was focused to $\sim$1 mm and incident at 45°. Target–substrate distance was $\sim$4 cm and deposition time was 1 h. Substrate temperatures were RT, 300, 500, and 800 °C ($\approx 5\ °C\ min^{-1}$ heating/cooling).

B. Structural characterization

Surface morphology and cross sections were examined by SEM; surface topography by AFM ($100 \times 100\ \mu m^2$ scans). Phase analysis used XRD (Cu Kα, 30 kV). Composition and Ca/P ratios were assessed by EDS and XPS. High-resolution XPS spectra (Ca 2p, P 2p, O 1s, C 1s) were charge-corrected to C 1s = 284.8 eV; fits used Shirley background and mixed Gaussian–Lorentzian line shapes with standard spin–orbit constraints. FTIR was used to identify hydroxyl and carbonate features where relevant.

C. TOF-SIMS depth profiling

Dual-beam TOF-SIMS was employed to probe through-thickness composition and the coating/substrate interface. Analyses covered $\sim 200 \times 200\ \mu m^2$ within a $\sim 500 \times 500\ \mu m^2$ sputter window using Cs^+ at 2 keV; profiles extended to $\sim$6.5 μm depth under UHV ($\sim 10^{-10}$ mbar). SIMS signals were used to track relative trends (e.g., C/CO_3^{2-}, O/H, and Ti/O) vs. temperature; absolute concentrations were not assigned without external normalization.

D. Protein attachment study

Protein adsorption and desorption behavior were evaluated using Bovine Serum Albumin (BSA) as a model protein to assess the bioactivity of the HA coatings. The experimental procedure for protein adsorption and desorption measurements, including sample preparation, incubation, and quantification steps, was identical to that described in Ref. 17. In the present work, these previously obtained experimental data were reanalyzed using Kramers' kinetic model to extract quantitative desorption rate constants and activation barriers associated with protein–surface interactions. This reanalysis provides a new theoretical interpretation of linking surface chemistry, deposition temperature, and protein binding stability.

III. RESULTS AND DISCUSSION

A. SEM-EDS analysis: Morphology and change in the Ca/P ratio

The SEM images and EDS spectra of HA thin films deposited onto titanium substrates, shown in Fig. 1, were analyzed to evaluate the surface morphology and elemental composition, along with stoichiometry. The presence of characteristic oxygen, calcium, and

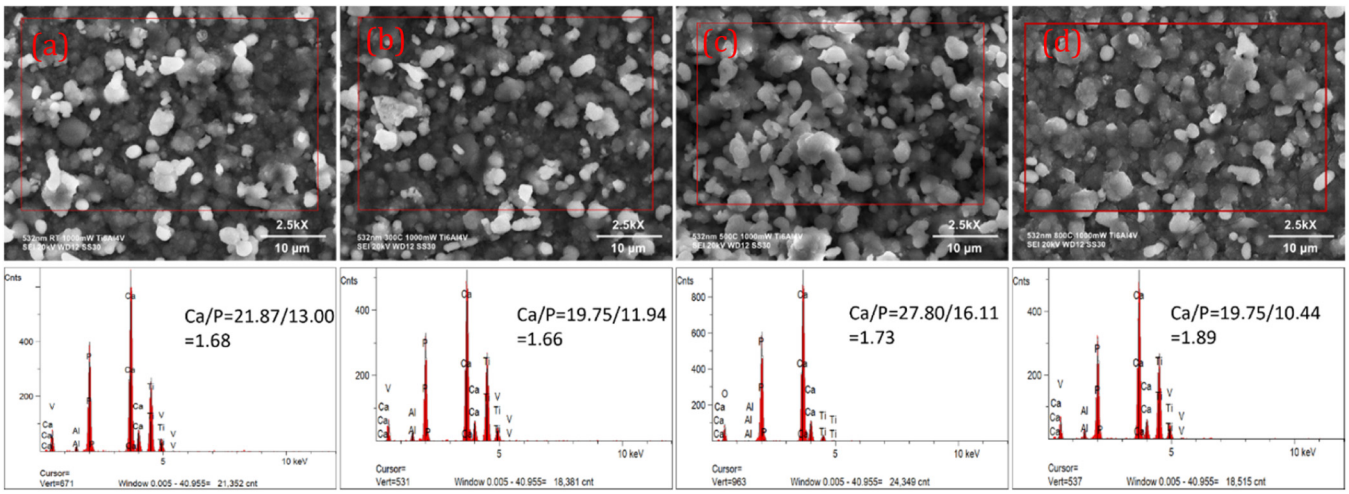

FIG. 1. EDS spectra of HA coatings deposited onto Ti6Al4V at various substrate temperatures: (a) RT, (b) 300, (c) 500, and (d) 800 °C.

phosphorus peaks originating from the target material could be seen.

The Ca/P ratio of the target was 1.67, corresponding to stoichiometric HA. Stoichiometric deposition was achieved at RT and 300 °C, as indicated in Fig. 1.

The thickness of thin films is of high importance in determining the fatigue life of biomedical implants. Previous studies have indicated that, for HA coatings, thicknesses up to 100 μm are preferred for enhancing mechanical fatigue resistance.[10,29,30] In our case, the film thickness was around 2.35 μm after 30 min deposition time. One advantage of PLD is that the thickness of the film can be easily controlled by varying laser parameters such as power, wavelength, and repetition rate. The deposition rate was calculated to be 78.33 nm/min. As observed in Figs. 2(a)–2(c), the HA coatings deposited at RT exhibit higher porosity and uncondensed particulates. In contrast, coatings obtained at elevated substrate temperatures display reduced porosity.

However, at a substrate temperature of 800 °C, a noticeable degradation of the film structure is evident. Figures 2(d)–2(f) present the AFM scans over a 100 × 100 μm^2 area. In the corners of each AFM scan, one can observe the corresponding surface roughness average (R_a) and root mean square roughness (R_q) values. The deposition performed at RT exhibited the highest surface roughness, followed by the coating obtained at 500 °C, while the sample deposited at 800 °C showed the lowest roughness values. This trend is consistent with expectations, as higher substrate temperatures provide increased surface mobility for adatoms and particulates, promoting film densification and structural reorganization. As a result, smoother and more crystalline films are formed at elevated deposition temperatures.

One of the key problems related to high-temperature deposition of HA is the deterioration of adhesion strength. It is well established that increasing the substrate temperature beyond a certain threshold can negatively impact the interfacial bonding between the HA coating and the metallic substrate. Several studies have reported reduced adhesion of HA coatings on Ti6Al4V and other metal surfaces at elevated temperatures.[31–33] This process is also evident in Fig. 2, where the HA deposition performed at the highest temperature exhibits structural discontinuities and loss of uniformity, indicative of compromised adhesion.

These observations are further supported by SIMS depth profiling, as shown in Fig. 4, which reveals the formation of a pronounced oxide layer at the HA coating–substrate interface at elevated substrate temperatures. The significant increase in oxygen signal intensity at the interface suggests extensive oxidation of the metallic surface, likely due to prolonged thermal exposure. This finding provides strong evidence of interfacial degradation and highlights the critical role of oxide layer formation in weakening the adhesion between the HA coating and the underlying Ti6Al4V substrate.

B. Protein desorption from HA surfaces

Protein adsorption and desorption play a crucial role in determining the biological performance of HA coatings.[34,35] Upon exposure to physiological environments, proteins rapidly adsorb onto the material surface, forming a dynamic interfacial layer that governs subsequent cellular responses, including adhesion, proliferation, and differentiation. The composition, conformation, and stability of this adsorbed protein layer are influenced by multiple surface characteristics, such as morphology, charge distribution, crystallinity, and chemical composition.[34] These surface properties are, in turn, strongly dependent on the deposition temperature and other processing parameters employed during film growth.[3–6,15,17,26] Protein adsorption–desorption behavior was reexamined using the BSA desorption dataset previously reported in Ref. 17, Fig. 3. In the present study, the time-dependent desorption curves were reanalyzed within the framework of Kramers' kinetic theory in order to extract quantitative descriptors of the desorption process and to relate these

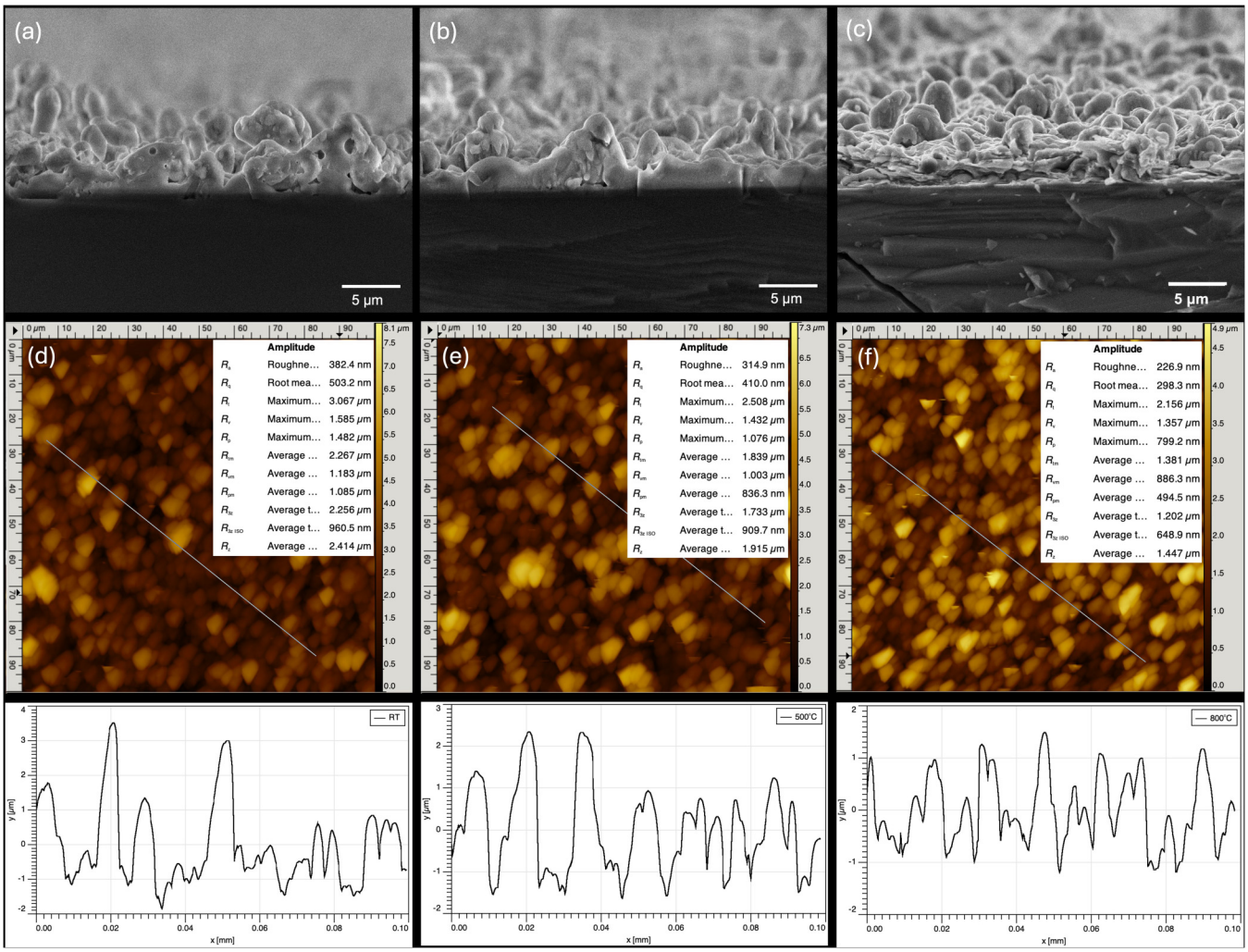

FIG. 2. Cross-sectional SEM images of HA coatings deposited onto Ti6Al4V at (a) RT, (b) 500, and (c) 800 °C. (d)–(f) corresponding top-view AFM scans over a 100 × 100 μm^2 area for the coatings shown in (a)–(c), respectively. The line profiles in each AFM scan illustrate the surface topography and roughness features of the films.

parameters directly to the deposition temperature–dependent evolution of the HA films.

For each temperature condition, the experimental desorption profiles were fitted to obtain characteristic time constants (τ), which represent the average time scale over which adsorbed proteins detach from the surface. The uncoated Ti6Al4V substrate exhibited the fastest desorption, with $\tau \approx 116 \pm 3$ h, consistent with its relatively low surface energy and limited density of hydroxyl and phosphate groups that promote protein anchoring. In contrast, HA coatings deposited at 500 °C showed the highest protein retention ($\tau \approx 147 \pm 2$ h), indicating the formation of a surface with optimal crystallinity and chemical functionality for stable protein attachment. Coatings produced at 800 °C displayed substantially reduced τ values ($\approx 81 \pm 1$ h), reflecting a marked decrease in protein–surface affinity.

Although the qualitative trends in protein retention were identified in the earlier study, the present work provides a new quantitative interpretation by linking the extracted τ values to thermally driven modifications in the HA film's structural and chemical characteristics. Specifically, application of Kramers' theory allows the desorption rate constant to be expressed in terms of an effective energy barrier, E_a, associated with protein detachment. Moderate deposition temperatures (300–500 °C) increase film density and crystallinity, thereby enhancing the number and stability of protein-binding sites such as surface hydroxyls. At higher temperatures (≥700–800 °C), however, dehydroxylation, phosphate loss, and partial phase decomposition, supported by SIMS, XPS, and XRD in Secs. III A–III C, reduce the availability of these chemical groups and disrupt the nanoscale topography that supports stable protein adsorption. These

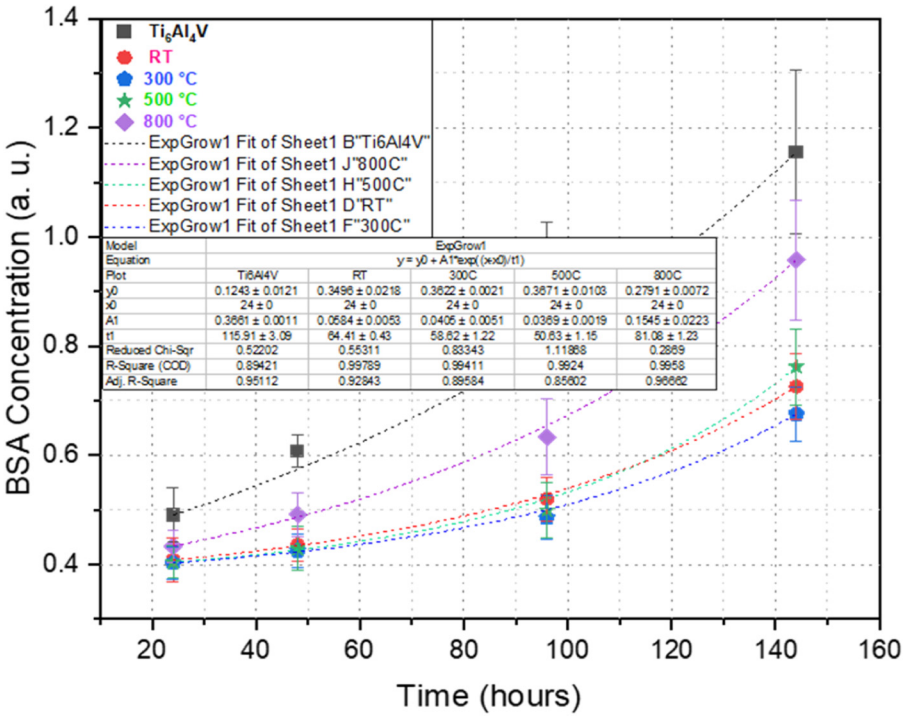

Model	ExpGrow1				
Equation	y = y0 + A1*exp((x-x0)/t1)				
Plot	Ti6Al4V	RT	300C	500C	800C
y0	0.1243 ± 0.0121	0.3496 ± 0.0218	0.3622 ± 0.0021	0.3671 ± 0.0103	0.2791 ± 0.0072
x0	24 ± 0	24 ± 0	24 ± 0	24 ± 0	24 ± 0
A1	0.3661 ± 0.0011	0.0584 ± 0.0053	0.0405 ± 0.0051	0.0369 ± 0.0019	0.1545 ± 0.0223
t1	115.91 ± 3.09	64.41 ± 0.43	58.62 ± 1.22	50.63 ± 1.15	81.08 ± 1.23
Reduced Chi-Sqr	0.52202	0.55311	0.83343	1.11868	0.2869
R-Square (COD)	0.89421	0.99789	0.99411	0.9924	0.9958
Adj. R-Square	0.95112	0.92843	0.89584	0.85602	0.96662

FIG. 3. BSA desorption rates from uncoated and HA-coated surfaces at different deposition temperatures. Data from Ref. 17 were reanalyzed using Kramers' kinetic. Adapted from Kylychbekov *et al.*, Coatings **13**, 1681 (2023). Copyright 2023 Author(s), licensed under a CC BY 4.0.

changes collectively lower the effective E_a, resulting in accelerated protein release.

Thus, by combining reanalyzed desorption data with a theoretical kinetic model, this study reveals a mechanistic connection between thermal processing, surface chemistry, and protein–surface interactions. The analysis demonstrates that intermediate deposition temperatures yield the most favorable balance between crystallinity and chemical stability, while excessive heating compromises bioactivity through reduced protein retention. This expanded interpretation represents a significant advance beyond the qualitative observations originally reported in Ref. 17, providing a deeper understanding of how processing conditions influence biological functionality in HA coatings.

C. SIMS investigation

To gain deeper insight into the decrease in coating adhesion observed at elevated substrate temperatures, as well as the corresponding increase in the Ca/P ratio identified through SEM (Fig. 2) and XPS analyses (Figs. 5–7), SIMS measurements were conducted.

SIMS is a valuable technique to determine elemental composition along the interface and thickness. Figure 4 presents the elemental distribution of C, CO_2, CO_3^{2-}, H, and O as a function of depth for coatings deposited at RT, 500, and 800 °C. Carbon content increases significantly with increasing deposition temperature, particularly at 800 °C, suggesting contamination or thermally induced reactions leading to higher incorporation of carbon-based species. Similarly, CO_2 and CO_3^{2-} concentrations rise, indicating carbonate substitution of phosphate (PO_4^{3-}) at high temperatures.

It should be noted that SIMS primarily provides qualitative information, and the absolute concentration of light elements such as carbon cannot be accurately determined without appropriate normalization—e.g., via electron microprobe analysis (EMPA), effective matrix factors (EMF), or other calibration protocols. In this study, SIMS data were therefore used to evaluate relative trends in elemental distribution as a function of temperature, rather than to extract absolute concentrations. Similar qualitative interpretations of carbon- and carbonate-related SIMS fragments in HA-based and CaP-based biomaterials have been reported in several recent works.

The observed increase in carbon- and carbonate-related secondary ion fragments with rising deposition temperature aligns with recent reports on carbon incorporation and interfacial modification in HA-based coatings and nanocomposites.[36–38] These findings support our interpretation that thermal exposure promotes carbonate substitution and induces structural evolution within HA coatings. This process is expected as HA undergoes thermal decomposition, leading to the replacement of phosphate groups with carbonate species.

The SIMS data also reveal that at low temperatures such as RT, the levels of C and CO_3^{2-} decrease significantly beyond a depth of 4 μm, indicating that the surface layer composition differs from the underlying material. This decrease in carbon content at greater depths could contribute to the observed changes in adhesion at higher deposition temperatures. Indeed, Cotell *et al.* have attributed similar degradation in adherence of HA coatings on Ti6Al4V to elevated substrate temperatures, especially noting a marked decline in adherence for coatings deposited above 600 °C.[39] This analysis

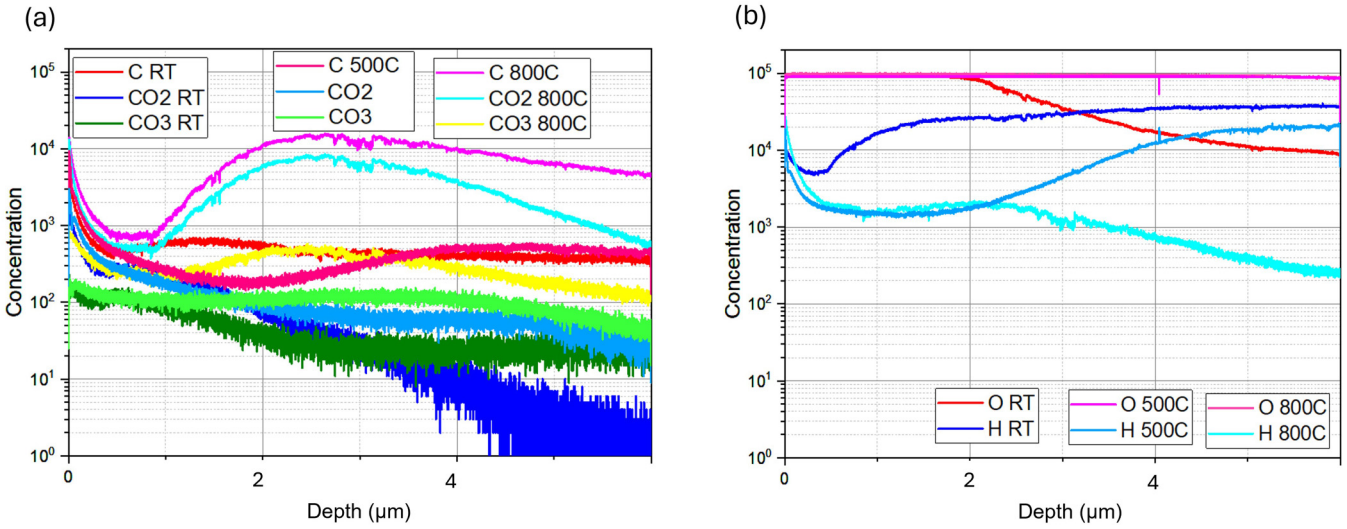

FIG. 4. SIMS elemental composition analysis of HA coatings across their thickness: (a) composition of C, CO_2, and CO_3^{2-} and (b) composition of O and H.

shows the importance of controlling deposition parameters to achieve coatings with desirable properties for specific biomedical applications.

It is also important to note that, despite the observed decrease in adherence at elevated temperatures—from 38–40 to 27 MPa the values remain well above the minimum threshold of 15 MPa required by ISO standards for HA coatings.[40] Overall, these findings are in agreement with previously reported results for HA and biologically derived- or doped-HA coatings deposited by PLD at 800 °C, reinforcing PLD as a desirable solution for achieving coatings with superior adherence[41,42] compared to plasma spraying[43] and mechanical properties comparable to those obtained by magnetron sputtering.[44]

Hydrogen content declines sharply with increasing substrate temperature, becoming nearly undetectable at 800 °C, supporting the hypothesis of dehydroxylation (loss of OH^- groups). Oxygen content remains relatively stable, but at higher depths, an increase is observed at high temperatures, likely due to oxide formation at the substrate–coating interface.

SIMS data at higher temperatures, particularly at 500 and 800 °C, reveal an increased abundance of C content and CO_3^{2-}. This observation aligns with the XPS analysis (Fig. 5), which indicates that at elevated temperatures, CO_3^{2-} groups replace PO_4^{3-} groups within the coating. Figure 4(b) reveals two additional significant findings. First, at 500 °C, the hydrogen content decreases significantly, and at 800 °C, it becomes nearly undetectable, suggesting that hydrogen evaporates from the surface at these high temperatures. *This loss of hydrogen could affect the chemical structure and stability of the coating.* Furthermore, SIMS data indicates that at temperatures exceeding 500 °C, the Ti6Al4V substrate begins to oxidize. This oxidation likely leads to an accumulation of oxide at the substrate-coating interface, which could contribute to the observed decline in adherence performance (see the supplementary material, as well as Cotell *et al.*,[11] which hypothesized the existence of oxide layer). This highlights the impact of temperature on the overall integrity of the coating. The thermal decomposition of HA is happening via two routes: dehydroxylation and phosphate group loss.

1. Dehydroxylation

Heating promotes dehydroxylation of HA [$Ca_{10}(PO_4)_6(OH)_2$], gradual loss of OH^- as H_2O, resulting in hydroxyl-deficient

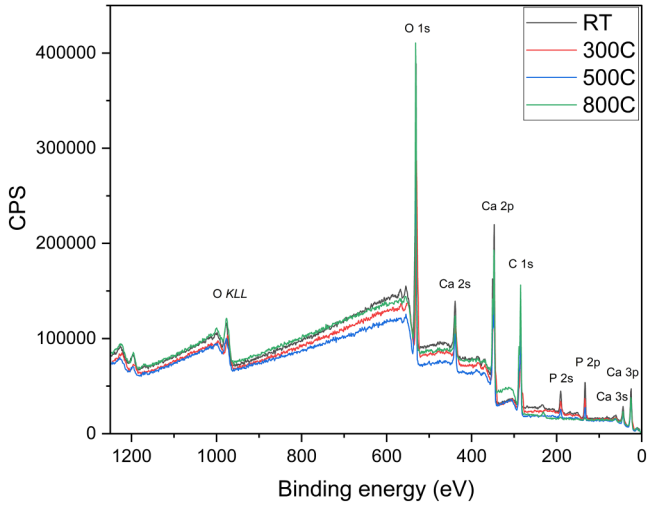

FIG. 5. XPS spectra of all samples from RT to 800 °C.

oxy-hydroxyapatite (OHA),

$$Ca_{10}(PO_4)_6(OH)_2 \rightarrow Ca_{10}(PO_4)_6(OH)_{2-2x}O_x\,\square_x + xH_2O(gas). \quad (1)$$

This constitutes the first step of thermal decomposition, as evidenced by FTIR and TGA investigations in the literature.[45,46] In agreement, our SIMS measurements [Fig. (4b)] reveal a sharp fall in hydrogen, approaching non-detectable levels at 800 °C. Although adding water vapor during PLD can partially restore OH^-, the effect is limited to ~400–700 °C.

2. Phosphate loss and carbonate substitution

Another process in the thermal decomposition of HA is phosphate loss. This can proceed via several mechanisms, including carbonate substitution,[47] conversion of HA to TCP, TTCP, and H_2O(gas),[48] and transformation of HA into TCP and CaO.[49] An example of phosphate loss by carbonate substitution is

$$Ca_{10}(PO_4)_6(OH)_2 + CO_2 \rightarrow Ca_{10}(PO_4)_6(CO_3) + H_2O(gas). \quad (2)$$

Our SIMS data show increasing signals from carbon- and CO_3^{2-}-containing fragments with temperature, while XPS reveals a simultaneous decrease in the P 2p intensity and an increase in the Ca/P ratio. Together, these trends point to carbonate substitution for PO_4^{3-} groups and partial thermal decomposition of HA at elevated temperatures.

D. XPS analysis

To further understand the elemental composition and chemical states of the coatings, XPS studies were performed (Fig. 5). To clarify the XPS results and ensure reproducibility, high-resolution scans were acquired for the Ca 2p, P 2p, O 1s, and C 1s core-level regions using Al Kα radiation (1486.6 eV).

All spectra were charge-corrected by referencing the C 1s peak at 284.8 eV and deconvoluted using a Shirley background and mixed Gaussian–Lorentzian line shapes, applying standard spin–orbit constraints where applicable.

Figure 5 shows the full XPS survey spectra, where the characteristic Ca, P, O, and C peaks of hydroxyapatite are observed in all coatings. The relative intensities of these peaks change systematically with temperature, providing the first indication of chemical modification. In particular, the Ca 2p and O 1s peaks remain prominent for all samples, while the P-related peaks (P 2p and P 2s) gradually decrease in intensity as the deposition temperature increases. This reduction becomes most pronounced in the 800 °C sample, suggesting phosphate loss and high-temperature degradation, consistent with the compositional trends revealed by SIMS and XRD. The increasing O—C=O contribution in the C 1s region also reflects enhanced carbonate incorporation at elevated temperatures. These survey spectra establish the overall chemical evolution of the films and motivate the detailed peak-fitting analysis presented in Figs. 6 and 7.

Figure 6 provides a closer examination of the temperature-dependent changes through deconvoluted P 2p and Ca 2p spectra. From RT to 500 °C, the P 2p doublet and Ca 2p peaks remain well defined with consistent component ratios, confirming preservation of the phosphate environment and stable Ca—O coordination. At 800 °C, however, the P 2p peak becomes strongly attenuated and broadened, indicating phosphate depletion, while the Ca 2p peak shows a stronger lower-binding-energy component associated with Ca-rich, partially decomposed species. These changes align with the disappearance of P 2s intensity observed in Fig. 5, reinforcing that phosphate loss becomes significant only at the highest temperature.

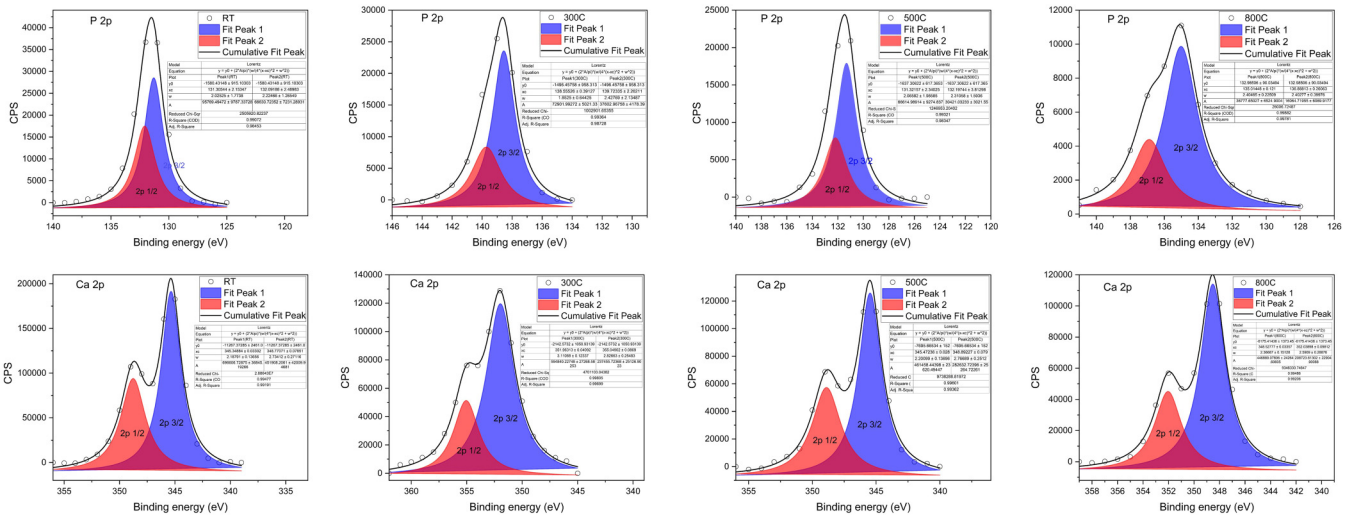

FIG. 6. Deconvoluted XPS spectra of the P 2p and Ca 2p regions for HA coatings deposited at RT, 300, 500, and 800 °C, highlighting temperature-dependent changes in phosphate and calcium bonding environments.

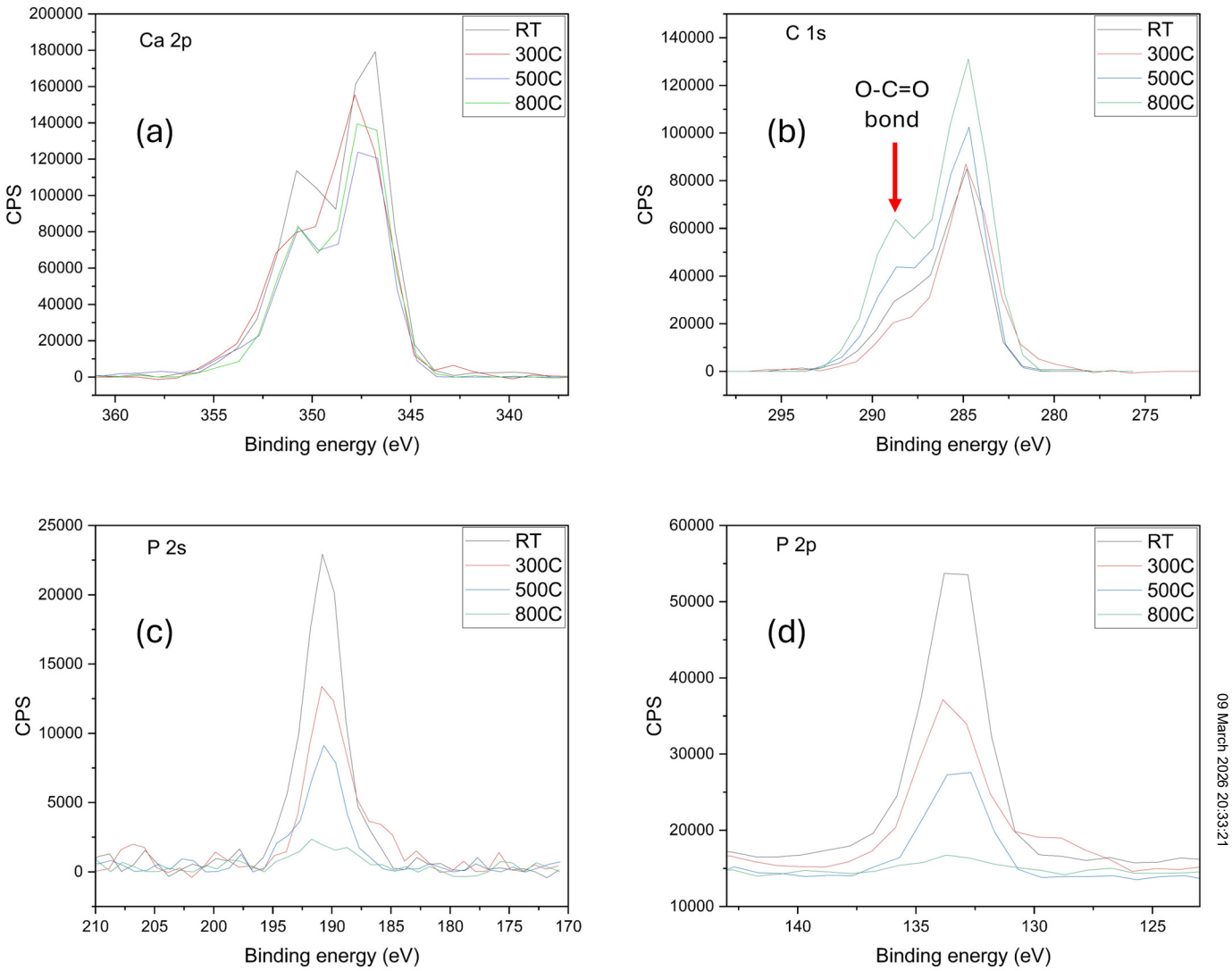

FIG. 7. XPS core-level spectra of hydroxyapatite coatings deposited at RT, 300, 500, and 800 °C, plotted for direct comparison: (a) Ca 2p, (b) P 2p and P 2s, (c) C 1s, and (d) O 1s regions. All spectra were acquired in the present study. References cited in the text are provided for interpretation and comparison of chemical trends only.

Figure 7 further highlights the evolution of the Ca 2p, P 2p, P 2s, and C 1s core levels overlaid for all temperatures. The data show that chemical stability is maintained up to ~500 °C, whereas coatings deposited at 800 °C undergo substantial dehydroxylation, carbonate substitution, and phosphate loss. The decrease in P 2p and P 2s signals directly suggests the removal of phosphorus from the coating. This process aligns with previous FTIR studies, which indicate that at higher substrate temperatures, phosphate groups evaporate from the coating, leading to a higher Ca/P ratio.[14,50]

The simultaneous increase in the intensity of C—C and C—O components in the C 1s spectrum indicates partial carbonization of the surface, along with the formation of carbon–oxygen functional groups. It is worthwhile to note that overall area of C 1s peak is increased as well, however, O—C=O part is more prominent, indicating a systematic rise in CO_3^{2-} carbonate content (see more detailed analysis: Fig. S10 in the supplementary material).

The reduction of the hydroxyl-related O 1s signal indicates progressive dehydroxylation, consistent with SIMS results showing hydrogen evaporation [Fig. 4(b)] and previous FTIR observations that OH^- groups are lost during high-temperature deposition.[51–53] By the principle of superposition, this suggests that the coating is undergoing carbonization, forming C—C and C—O bonds. This phenomenon was well explained by Forero-Sossa *et al.*,[50] who

TABLE I. XPS peak areas: Measured and sensitivity-factor-corrected values.

			RT	300 °C	500 °C	800 °C
Ca 2p	Ca 2p 3/2	Obtained area	696 607	594 840	461 458	446 889
		Sensitivity Factor	3.35	3.35	3.35	3.35
		Corrected area	207 942.3881	177 564.1791	137 748.6567	133 399.7015
	Ca 2p 1/2	Obtained area	451 908	237 456	282 633	208 723
		Sensitivity Factor	1.72	1.72	1.72	1.72
		Corrected area	262 737.2093	138 055.814	164 321.5116	121 350.5814
	Total		470 679.5974	315 619.9931	302 070.1683	254 750.2829
P 2p	P 2p 3/2	Obtained area	95 770	72 902	66 615	36 778
		Sensitivity Factor	0.789	0.789	0.789	0.789
		Corrected area	121 381.4956	92 397.972 12	84 429.657 79	46 613.434 73
	P 2p 1/2	Obtained area	66 631	37 603	30 421	16 065
		Sensitivity Factor	0.403	0.403	0.403	0.403
		Corrected area	165 337.469	93 307.692 31	75 486.352 36	39 863.523 57
	Total		286 718.9645	185 705.6644	159 916.0102	86 476.9583
Ca/P ratio: Ca 2p/P 2p			1.641 606 087	1.699 571 168	1.888 930 121	2.945 874 692

demonstrated that at sintering temperatures exceeding 1000 °C, FTIR peaks confirmed the replacement of phosphate groups with carbonate groups.

Quantitative XPS analysis was performed using the measured peak areas and sensitivity factors for Ca 2p and P 2p (Table I). The resulting Ca/P ratios increase systematically with deposition temperature, from 1.64 at RT to 1.70 at 300 °C, 1.89 at 500 °C, and 2.95 at 800 °C. Values near the stoichiometric ratio of 1.67 are preserved only up to ~300 °C, indicating that the phosphate framework remains largely intact at lower temperatures. Above 500 °C, the Ca/P ratio increases sharply, consistent with temperature-induced phosphate loss and dehydroxylation. The exceptionally high Ca/P ratio at 800 °C agrees with the near disappearance of the P 2p signal and the emergence of TTCP in XRD, confirming substantial HA decomposition at elevated temperatures.

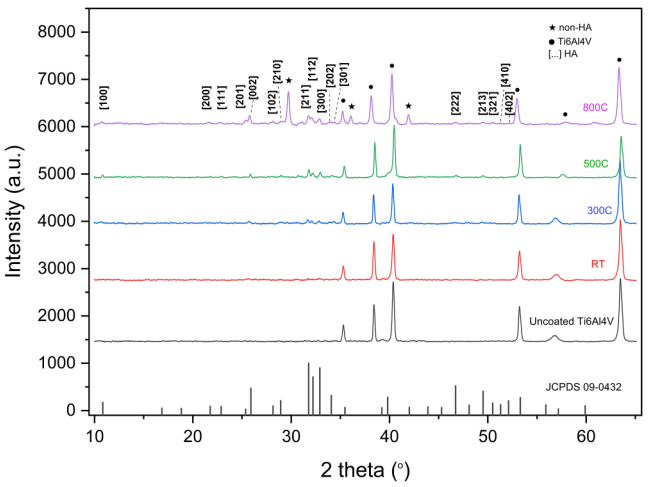

FIG. 8. X-ray diffractograms of coatings synthesized on Ti6Al4V from RT to 800 °C.

E. XRD analysis

To corroborate the temperature-dependent chemical changes identified by SIMS and XPS, x-ray diffraction (XRD) patterns were also collected for HA coatings deposited at RT, 300, 500, and 800 °C, as shown in Fig. 8. From RT to 500 °C, all patterns exhibit the characteristic reflections of crystalline HA (JCPDS 09-0432), indicating phase retention within this window. Peaks sharpening at 500 °C are consistent with enhanced crystallinity and the surface densification discussed above.

At 800 °C, additional reflections appear that correspond to tetracalcium phosphate (TTCP), a hallmark of high-temperature HA decomposition, in agreement with the increased Ca/P ratio and phosphate loss observed by SIMS and XPS investigations. Peaks from the Ti6Al4V substrate are also evident, likely due to partial thinning or disruption of the coating at this temperature, consistent with the adhesion loss reported in Ref. 17. These results demonstrate that HA remains structurally stable up to approximately 500 °C, whereas deposition at 800 °C initiates decomposition (HA → TTCP), supporting the mechanistic interpretation derived from chemical depth profiling.

Overall, the XRD results show that temperature strongly influences HA stability: moderate heating (~500 °C) enhances crystallinity with minimal chemical alteration, whereas higher temperatures trigger dehydroxylation, phosphate loss, and secondary-phase formation, leading to diminished bioactivity and weaker adhesion.

IV. CONCLUSIONS

We investigated the chemical composition, structural stability, and degradation mechanisms of hydroxyapatite (HA) coatings

deposited by pulsed laser deposition (PLD) from room temperature to 800 °C. XPS and SIMS analyses reveal that elevated deposition temperatures lead to the loss of OH^- and PO_4^{3-} groups, an increase in the Ca/P ratio, and the formation of an interfacial oxide layer at the coating–substrate interface. These chemical and structural changes—particularly dehydroxylation and carbonate substitution—correlate with reduced adhesion strength and diminished bioactivity.

Surface morphology analysis by SEM and AFM indicates progressive densification and smoothing with increasing temperature; however, structural degradation becomes evident at 800 °C. Importantly, a Kramers-type kinetic reanalysis of previously obtained BSA desorption data, considered in conjunction with earlier cell-proliferation results, consistently identifies ∼500 °C as the optimal processing temperature. At this temperature, a favorable balance between crystallinity and surface chemistry promotes stable protein attachment. In contrast, higher deposition temperatures accelerate protein desorption, likely due to the loss of active binding sites.

In summary, our results identify two principal thermal-degradation pathways—dehydroxylation and phosphate loss/carbonate substitution—and highlight interfacial oxidation as a critical factor contributing to adhesion decline. Despite degradation at higher temperatures, the measured adhesion strength remains above the ISO threshold of 15 MPa, supporting the practical viability of PLD for biomedical coating applications. Future work will focus on mitigating high-temperature effects through controlled water-vapor enrichment and the introduction of interfacial buffer layers, as well as on validating the proposed kinetic framework using new protein-specific adsorption assays.

SUPPLEMENTARY MATERIAL

The supplementary material includes additional experimental data and detailed analyses supporting the results presented in the main text. Specifically, detailed x-ray photoelectron spectroscopy (XPS) analyses are provided, including Ca 2p and P 2p peak fitting, Ca/P ratio calculations, uncertainty and error propagation analysis, and C 1s peak evolution as a function of deposition temperature. These data provide further insight into the compositional variation, interfacial adhesion, and chemical states of the HA coatings.

ACKNOWLEDGMENTS

This project is fully supported by Kentucky Biomedical Research Infrastructure Network and INBRE (KBRIN) No. 5P20GM 103436-23 and NSF MRI (Award No. 1920069), KY NSF EPSCoR RA (No. 3200002692-23-011). L.D. acknowledges the support given by the Romanian Ministry of Education and Research, under Romanian National Nucleu Program LAPLAS VII—Contract No. 30N/2023.

AUTHOR DECLARATIONS

Conflict of Interest

The authors have no conflicts to disclose.

Author Contributions

Salizhan Kylychbekov: Formal analysis (equal); Investigation (equal); Writing – original draft (equal); Writing – review & editing (equal). **Bektur Abdisatarov:** Formal analysis (equal); Writing – original draft (equal); Writing – review & editing (equal). **Yaran Allamyradov:** Conceptualization (equal); Formal analysis (equal); Writing – original draft (equal); Writing – review & editing (equal). **Berdimyrat Annamuradov:** Formal analysis (equal); Writing – original draft (equal); Writing – review & editing (equal). **Liviu Duta:** Data curation (equal); Formal analysis (equal); Funding acquisition (supporting); Writing – original draft (equal); Writing – review & editing (equal). **Ali Oguz Er:** Conceptualization (equal); Formal analysis (lead); Funding acquisition (lead); Investigation (lead); Writing – original draft (equal); Writing – review & editing (equal).

DATA AVAILABILITY

The data that support the findings of this study are available from the corresponding author upon reasonable request.

REFERENCES

[1]H. Breme, V. Biehl, N. Reger, and E. Gawalt, " Metallic biomaterials: Introduction," in *Handbook of Biomaterial Properties*, edited by W. Murphy, J. Black, and G. Hastings (Springer New York, New York, 2016), Chap. 1a, pp. 151–158. ISBN 978-1-4939-3305-1.
[2]Q. Chen and G. A. Thouas, "Metallic implant biomaterials," Mater. Sci. Eng. R Rep. **87**, 1–57 (2015).
[3]A. Bandyopadhyay, I. Mitra, S. B. Goodman, M. Kumar, and S. Bose, "Improving biocompatibility for next generation of metallic implants," Prog. Mater. Sci. **133**, 101053 (2023).
[4]N. Espallargas, C. Torres, and A.I. Muñoz, "A metal Ion release study of CoCrMo exposed to corrosion and tribocorrosion conditions in simulated body fluids," Wear **332–333**, 669–678 (2015).
[5]P. Choudhury and D. C. Agrawal, "5 - hydroxyapatite (HA) coatings for biomaterials," in *Nanomedicine*, edited by T. J. Webster (Woodhead Publishing, 2012), pp. 84–127.
[6]I. N. Mihailescu, S. Lamolle, G. Socol, F. Miroiu, F. J. Roenold, A. Bigi *et al.*, "*In vivo* tensile test of biomimetic titanium implants pulsed laser coated with nanostructured calcium phosphate thin films," J. Optoelectron. Adv. Mater. **2**, 337–341 (2008), see http://hdl.handle.net/11585/67930.
[7]D.-E. Radulescu, O. R. Vasile, E. Andronescu, and A. Ficai, "Latest research of doped hydroxyapatite for bone tissue engineering," Int. J. Mol. Sci. **24**, 13157 (2023).
[8]M. Kumar, R. Kumar, and S. Kumar, "Coatings on orthopedic implants to overcome present problems and challenges: A focused review," Mater. Today Proc. **45**, 5269–5276 (2021).
[9]H. Pelletier, A. Carradò, J. Faerber, and I. Mihailescu, "Microstructure and mechanical characteristics of hydroxyapatite coatings on Ti/TiN/Si substrates synthesized by pulsed laser deposition," Appl. Phys. A **102**, 629–640 (2011).
[10]C. Gherde, P. Dhatrak, S. Nimbalkar, and S. Joshi, "A comprehensive review of factors affecting fatigue life of dental implants," Mater. Today Proc. **43**, 1117–1123 (2021).
[11]C. M. Cotell, D. B. Chrisey, K. S. Grabowski, J. A. Sprague, and C. R. Gossett, "Pulsed laser deposition of hydroxylapatite thin films on Ti-6Al-4V," J. Appl. Biomater. **3**, 87–93 (1992).
[12]J. M. Fernández-Pradas, L. Clèries, G. Sardin, and J. L. Morenza, "Hydroxyapatite coatings grown by pulsed laser deposition with a beam of 355 Nm wavelength," J. Mater. Res. **14**, 4715–4719 (1999).

[13]T. Smausz, B. Hopp, H. Huszár, Z. Tóth, and G. Kecskeméti, "Pulsed laser deposition of bioceramic thin films from human tooth," Appl. Phys. A **79**, 1101–1103 (2004).
[14]H. Zeng and W. R. X. P. S. Lacefield, "EDX and FTIR analysis of pulsed laser deposited calcium phosphate bioceramic coatings: The effects of various process parameters," Biomaterials **21**, 23–30 (2000).
[15]G. P. Dinda, J. Shin, and J. Mazumder, "Pulsed laser deposition of hydroxyapatite thin films on Ti–6Al–4V: Effect of heat treatment on structure and properties," Acta Biomater. **5**, 1821–1830 (2009).
[16]L. Clèries, J. M. Fernández-Pradas, G. Sardin, and J. L. Morenza, "Dissolution behaviour of calcium phosphate coatings obtained by laser ablation," Biomaterials **19**, 1483–1487 (1998).
[17]S. Kylychbekov, Y. Allamyradov, Z. Khuzhakulov, I. Majidov, S. Banga, J. Ben Yosef, L. Duta, and A. O. Er, "Bioactivity and mechanical properties of hydroxyapatite on Ti6Al4V and Si(100) surfaces by pulsed laser deposition," Coatings **13**, 1681 (2023).
[18]C. F. Koch, S. Johnson, D. Kumar, M. Jelinek, D. B. Chrisey, A. Doraiswamy, C. Jin, R. J. Narayan, and I. N. Mihailescu, "Pulsed laser deposition of hydroxyapatite thin films," Gener. Biomater. **27**, 484–494 (2007).
[19]P. Ducheyne, S. Radin, and L. King, "The effect of calcium phosphate ceramic composition and structure on *in vitro* behavior. I. Dissolution," J. Biomed. Mater. Res. **27**, 25–34 (1993).
[20]C. P. A. T. Klein, J. M. A. de Blieck-Hogemrst, J. G. C. Wolket, and K. de Groot, "Studies of the solubility of different calcium phosphate ceramic particles *in vitro*," Biomaterials **11**, 509–512 (1990).
[21]R. Z. LeGeros, "Biodegradation and bioresorption of calcium phosphate ceramics," Clin. Mater. **14**, 65–88 (1993).
[22]International Organization for Standardization, Implants for surgery—Hydroxyapatite—Part 2: Coatings of hydroxyapatite, ISO 13779-2 (2018).
[23]I. Mihailescu, S. taxt-lamolle, G. Socol, F. Miroiu, H. J. Roenold, A. Bigi, I. Mayer, F. Cuisinier, and S. Lyngstadaas, "*In vivo* tensile tests of biomimetic titanium implants pulsed laser coated with nanostructured calcium phosphate thin films," Optoelectron. Adv. Mater. Rapid Commun. **2**, 337–341 (2008).
[24]L. Duta, "*In vivo* assessment of synthetic and biological-derived calcium phosphate-based coatings fabricated by pulsed laser deposition: A review," Coatings **11**, 99 (2021).
[25]L. Ma, M. Li, S. Komasa, S. Hontsu, Y. Hashimoto, J. Okazaki, and K. Maekawa, "Effect of Er:YAG pulsed laser-deposited hydroxyapatite film on titanium implants on M2 macrophage polarization *in vitro* and osteogenesis *in vivo*," Int. J. Mol. Sci. **25**, 349 (2024).
[26]B. Beig, U. Liaqat, M. F. K. Niazi, I. Douna, M. Zahoor, and M. B. K. Niazi, "Current challenges and innovative developments in hydroxyapatite-based coatings on metallic materials for bone implantation: A review," Coatings **10**, 1249 (2020).
[27]L. Duta and A. C. Popescu, "Current status on pulsed laser deposition of coatings from animal-origin calcium phosphate sources," Coatings **9**, 335 (2019).
[28]A. C. Parau, C. M. Cotrut, P. Guglielmi, A. Cusanno, G. Palumbo, M. Dinu, G. Serratore, G. Ambrogio, D. M. Vranceanu, and A. Vladescu, "Deposition temperature effect on sputtered hydroxyapatite coatings prepared on AZ31B alloy substrate," Ceram. Int. **48**, 10486–10497 (2022).
[29]A. K. Lynn and D. L. DuQuesnay, "Hydroxyapatite-coated Ti–6Al–4V: Part 1: The effect of coating thickness on mechanical fatigue behaviour," Biomaterials **23**, 1937–1946 (2002).
[30]H. Akebono, J. Komotori, and H. Suzuki, "The effect of coating thickness on fatigue properties of steel thermally sprayed with ni-based self-fluxing alloy," Int. J. Mod. Phys. B **20**, 3599–3604 (2006).
[31]K. K. Saju, R. Reshmi, N. H. Jayadas, J. James, and M. K. Jayaraj, "Polycrystalline coating of hydroxyapatite on TiAl6V4 implant material grown at lower substrate temperatures by hydrothermal annealing after pulsed laser deposition," Proc. Inst. Mech. Eng. [H] **223**, 1049–1057 (2009).
[32]J. M. Fernández-Pradas, M. V. Garcı´a-Cuenca, L. Clèries, G. Sardin, and J. L. Morenza, "Influence of the interface layer on the adhesion of pulsed laser deposited hydroxyapatite coatings on titanium alloy," Appl. Surf. Sci. **195**, 31–37 (2002).
[33]A. C. Parau, M. Dinu, C. M. Cotrut, I. Pana, D. M. Vranceanu, L. R. Constantin, G. Serratore, I. M. Marinescu, C. Vitelaru, G. Ambrogio *et al.*, "Effect of deposition temperature on the structure, mechanical, electrochemical evaluation, degradation rate and peptides adhesion of Mg and Si-doped hydroxyapatite deposited on AZ31B alloy," Coatings **13**, 591 (2023).
[34]R. B. Heimann, "Plasma-sprayed osseoconductive hydroxylapatite coatings for endoprosthetic hip implants: Phase composition, microstructure, properties, and biomedical functions," Coatings **14**, 787 (2024).
[35]R. Kimura, D. Noda, Z. Liu, W. Shi, R. Akutsu, and M. Tagaya, "Biological surface layer formation on bioceramic particles for protein adsorption," Biomimetics **9**, 347 (2024).
[36]M. Davlet, K. Smyrnova, and A. Pogrebnjak, "Advanced biomaterials in tissue engineering: A critical review of nanocomposites based on bacterial cellulose, MXenes, hydroxyapatite, and metal particles for regenerative medicine," Adv. Colloid Interface Sci. **345**, 103634 (2025).
[37]A. Myakinin, A. Turlybekuly, A. Pogrebnjak, A. Mirek, M. Bechelany, I. Liubchak, O. Oleshko, Y. Husak, V. Korniienko, K. Leśniak-Ziółkowska *et al.*, "*In vitro* evaluation of electrochemically bioactivated Ti6Al4V 3D porous scaffolds," Mater. Sci. Eng. C **121**, 111870 (2021).
[38]A. Turlybekuly, A. D. Pogrebnjak, L. F. Sukhodub, L. B. Sukhodub, A. S. Kistaubayeva, I. S. Savitskaya, D. H. Shokatayeva, O. V. Bondar, Z. K. Shaimardanov, S. V. Plotnikov *et al.*, "Synthesis, characterization, *in vitro* biocompatibility and antibacterial properties study of nanocomposite materials based on hydroxyapatite-biphasic ZnO micro- and nanoparticles embedded in alginate matrix," Mater. Sci. Eng. C **104**, 109965 (2019).
[39]C. M. Cotell, "Pulsed laser deposition and processing of biocompatible hydroxylapatite thin films," Appl. Surf. Sci. **69**, 140–148 (1993).
[40]International Organization for Standardization, Implants for surgery—Hydroxyapatite—Part 2: Thermally sprayed coatings of hydroxyapatite, ISO 13779-22018 (2018).
[41]L. Duta, N. Mihailescu, A. C. Popescu, C. R. Luculescu, I. N. Mihailescu, G. Çetin, O. Gunduz, F. N. Oktar, A. C. Popa, A. Kuncser *et al.*, "Comparative physical, chemical and biological assessment of simple and titanium-doped ovine dentine-derived hydroxyapatite coatings fabricated by pulsed laser deposition," Appl. Surf. Sci. **413**, 129–139 (2017).
[42]L. Duta, G. E. Stan, G. Popescu-Pelin, I. Zgura, M. Anastasescu, and F. N. Oktar, "Influence of post-deposition thermal treatments on the morpho-structural, and bonding strength characteristics of lithium-doped biological-derived hydroxyapatite coatings," Coatings **12**, 1883 (2022).
[43]F. J. Garcia-Sanz, M. B. Mayor, J. L. Arias, J. Pou, B. Leon, and M. Perez-Amor, "Hydroxyapatite coatings: A comparative study between plasma-spray and pulsed laser deposition techniques," J. Mater. Sci. Mater. Med. **8**, 861–865 (1997).
[44]V. Nelea, C. Morosanu, M. Iliescu, and I. N. Mihailescu, "Hydroxyapatite thin films grown by pulsed laser deposition and radio-frequency magnetron sputtering: Comparative study," Appl. Surf. Sci. **228**, 346–356 (2004).
[45]P. E. Wang and T. K. Chaki, "Sintering behaviour and mechanical properties of hydroxyapatite and dicalcium phosphate," J. Mater. Sci. Mater. Med. **4**, 150–158 (1993).
[46]M. Markovic, B. O. Fowler, and M. S. Tung, "Preparation and comprehensive characterization of a calcium hydroxyapatite reference material," J. Res. Natl. Inst. Stand. Technol. **109**, 553 (2004).
[47]J. L. Arias, F. J. Garcı´a-Sanz, M. B. Mayor, S. Chiussi, J. Pou, B. León, and M. Pérez-Amor, "Physicochemical properties of calcium phosphate coatings produced by pulsed laser deposition at different water vapour pressures," Biomaterials **19**, 883–888 (1998).
[48]S.-F. Ou, S.-Y. Chiou, and K.-L. Ou, "Phase transformation on hydroxyapatite decomposition," Ceram. Int. **39**, 3809–3816 (2013).
[49]J. Zhou, X. Zhang, J. Chen, S. Zeng, and K. De Groot, "High temperature characteristics of synthetic hydroxyapatite," J. Mater. Sci. Mater. Med. **4**, 83–85 (1993).
[50]P. A. Forero-Sossa, J. D. Salazar-Martínez, A. L. Giraldo-Betancur, B. Segura-Giraldo, and E. Restrepo-Parra, "Temperature effect in

physicochemical and bioactive behavior of biogenic hydroxyapatite obtained from porcine bones," Sci. Rep. **11**, 11069 (2021).
[51]C.-J. Liao, F.-H. Lin, K.-S. Chen, and J.-S. Sun, "Thermal decomposition and reconstitution of hydroxyapatite in air atmosphere," Biomaterials **20**, 1807–1813 (1999).
[52]G. Muralithran and S. Ramesh, "The effects of sintering temperature on the properties of hydroxyapatite," Ceram. Int. **26**, 221–230 (2000).
[53]R. K. Singh, F. Qian, V. Nagabushnam, R. Damodaran, and B. M. Moudgil, "Excimer laser deposition of hydroxyapatite thin films," Biomaterials **15**, 522–528 (1994).